Experimental report

19/02/2019

Proposal: **5-53-278** **Council:** 4/2017

Title: Magnetic diffuse scattering in thenew Gd-pyrochlore antiferromagnet - Gd2Pt2O7

Research area: Physics

This proposal is a new proposal

Main proposer: **John Ross STEWART**

Experimental team: Philip WELCH
John Ross STEWART

Local contacts: Lucile MANGIN-THRO
Andrew WILDES

Samples: 160GdPt2O7

Instrument	Requested days	Allocated days	From	To
D7	5	5	21/03/2018	26/03/2018

Abstract:

We propose to characterise the magnetic ground state structure and the paramagnetic diffuse scattering in a newly synthesised (isotopically enriched) Gd-pyrochlore sample, Gd2Pt2O7. This displays a strong 1st order anomaly in the heat capacity at low temperatures (1.6K) that is consistent with a transition to a "Palmer-Chalker" state, and with a gapped excitation spectrum. Orbital chemistry associated with the Pt ions leads to possible new exchange pathways in this system, which are not present in the stannate or the titanate Gd-pyrochlores. Measurements of the diffuse scattering in the paramagnetic regime will allow us to test this hypothesis, and extract the dominant exchanges. We ask for 5 days on D7 to complete this study.

Magnetic diffuse scattering in the Gd-pyrochlore antiferromagnet – $Gd_2Pt_2O_7$

Philip G Welch,[1,2] Wei-Tin Chen,[3] Jason S Gardner,[3] Andrew R Wildes,[4] Joseph A M Paddison,[5] Andrew L Goodwin,[1] and J Ross Stewart[6]

[1] *Inorganic Chemistry Laboratory, University of Oxford, South Parks Road, Oxford, OX1 3QR*
[2] *ISIS Facility, Rutherford Appleton Laboratory, Harwell Campus, Didcot, OX11 0QX, United Kingdom*
[3] *Centre for Condensed Matter Sciences, National Taiwan University, Taipei, 10617, Taiwan*
[4] *Institut Max von Laue-Paul Langevin, F-38042 Grenoble 9, France*
[5] *Churchill College, University of Cambridge, Storey's Way, Cambridge, CB3 0DS, United Kingdom*
[6] *ISIS Neutron and Muon Facility, Science and Technology Facilities Council, Rutherford Appleton Laboratory, Didcot, OX11 0QX, United Kingdom*

(Dated: January 30, 2019)

$Gd_2Pt_2O_7$ is a recently reported member of the gadolinium pyrochlore family and is a good example of an antiferromagnetic Heisenberg-spin system. Previous reports have presented the bulk characterisation of this compound, and have predicted that, in spite of the 160% increase in T_N relative to $Gd_2Sn_2O_7$, the underlying interactions are relatively similar. We present the first neutron diffraction measurements of isotope enriched $^{160}Gd_2Pt_2O_7$. Our diffraction data show that the magnetically ordered state below $T_N = 1.6$ K is the so-called Palmer-Chalker state — a coplanar, $k = (000)$, antiferromagnet. Above the ordering temperature, we investigate the correlated paramagnetic regime, and determine that relative to $Gd_2Sn_2O_7$, the cross-hexagon (J_{3a}) exchange interaction is significantly stronger due to the superexchange pathways introduced due to the empty Pt^{4+} e_g orbitals.

I. INTRODUCTION

The pyrochlore lattice – comprised of corner-sharing tetrahedra – has commonly been studied as an archetypal example of a three-dimensionally frustrated system. Geometrical frustration, defined as the inability of a system to simultaneously satisfy all of its magnetic interactions, provides a route to potentially access a variety of magnetic states, from spin-liquids [1] to complex ordered structures [2, 3], due to the macroscopic degeneracy of the magnetic ground state. It is this degeneracy which serves to suppress the magnetic ordering temperature (T_N) below the Curie-Weiss temperature (θ_{CW}); which defines the net strength of the magnetic interactions. One measure of the degree of geometrical frustration in a system is the frustration parameter: $f = \frac{|\theta_{CW}|}{T_N}$. A frustration parameter of $f > 10$ generally indicates a highly frustrated material, while a value $f > 100$ would be indicative of a potential spin-liquid candidate. In a model system with only nearest-neighbour, antiferromagnetic, interactions on a perfect pyrochlore lattice, we would expect a spin-liquid ground state, due to the large degree of frustration [4, 5]. It is perturbations to this simple nearest-neighbour exchange – such as further neighbour interactions, dipolar exchange, or single-ion anisotropies – which cause most real systems to enter long-range ordered states at finite temperatures.

$Gd_2Pt_2O_7$ (GPO) is an interesting example where a combination of nearest-, next-nearest-, and dipolar-interactions, as well as single-ion physics, serve to relieve the frustration and give rise to long-range magnetic order at accessible temperatures. $Gd_2Pt_2O_7$ crystallises in the cubic, $Fd\bar{3}m$, space group, with $a = 10.26$ Å at room temperature [6, 7], and forms a pyrochlore network of corner-sharing tetrahedra, with a number of dominant exchange pathways, as shown in Figure 1. In the cubic pyrochlore system, there are two third neighbour interaction pathways at the same separation — one which occurs parallel to J_1, and one which crosses the hexagon formed due to corner-sharing tetrahedra.

In related, highly frustrated, materials, the temperature range just above the magnetic ordering temperature has been of significant interest, and it has been possible to observe a 'cooperative paramagnet' state over the temperature range $T_N < T \lesssim |\theta_{CW}|$ ($\theta_{CW} = -9.4(1)$ K) [6, 8]. In contrast with other Gd pyrochlores, GPO orders at $T_N = 1.6$ K, an ~60% enhancement relative to both $Gd_2Sn_2O_7$ (GSO) ($T_N = 1.0$ K) and $Gd_2Ti_2O_7$ (GTO) ($T_{N1} = 1.0$ K) [6]. Due to similarities in both the heat capacity and magnetic susceptibility measurements of GPO and GSO, it is suggested by Hallas *et al.* that GPO will also order into the so-called Palmer-Chalker ($\mathbf{k} = (0\,0\,0)$) state.

In this report we present the results of polarised neutron scattering experiments for both the ordered ($T = 50$ mK) and correlated paramagnetic ($T = 1.8$ K) regimes of GPO. We find that the low-temperature state of GPO is the coplanar, antiferromagnetic, Palmer-Chalker state with a $\mathbf{k} = (0\,0\,0)$ ordering vector. Above the magnetic transition, significant diffuse magnetic scattering is observed, implying that there is a strongly correlated paramagnetic state, which persists above T_N. Our analysis of this state reveals that the cross-hexagon magnetic interactions are significantly enhanced relative to GSO, possibly due to the nature of the superexchange pathways mediated by Pt^{4+}. In Section II, we introduce the methods used to analyse our collected data; in Section III our main results are presented and discussed; and in Section IV we give our conclusions.

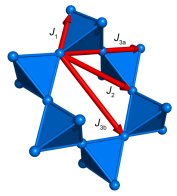

FIG. 1. The arrangement of Gd^{3+} ions (blue circles) in $Gd_2Pt_2O_7$. The network of corner-sharing tetrahedra is illustrated in blue. Principal exchange interaction pathways are shown in red, demonstrating the difference between the two next-nearest-neighbour interactions: the 'through-Gd' J_{3a} and the 'cross-hexagon' J_{3b}.

II. METHODS

A. Experimental Details

The sample used in our neutron scattering experiments was synthesised using high-pressure, high-temperature (HPHT) techniques. A stoichiometric amount of starting materials was well mixed and filled into a gold capsule, and subsequently treated at 1100°C and 6 GPa in a DIA-type cubic anvil high pressure apparatus.

$$^{160}Gd_2O_3 + 2PtO_2 \rightarrow Gd_2Pt_2O_7. \quad (1)$$

Certain pyrochlores require HPHT syntheses due to the size mismatch of the relative ionic radii of A^{3+} and B^{4+}; high pressures are required for PtO_2 to prevent it from melting at temperatures lower than required for the solid-state synthesis. Neutron scattering data have been collected on a polycrystalline sample of GPO (0.21 g) across a wide temperature range, from 50 mK to 200 K. These measurements were performed on the D7 diffuse scattering spectrometer at the ILL, Grenoble, using an incident neutron wavelength of 4.86 Å [9, 10]. D7 is able to perform xyz polarisation analysis and has support for a $^3He/^4He$ dilution refrigerator, both of which were used in our experiment. This incident wavelength and the solid angle covered by 132 ^3He detectors give access to a usable Q-range of $0.15 \leq Q \leq 2.5$ Å^{-1}, with the low Q_{min} allowing determination of relatively long-range magnetic interactions. xyz polarisation analysis enables the separation of the magnetic scattering from the nuclear and the spin-incoherent scattering contributions using the scattering cross sections given by Schärpf *et al.* [11]. The collected data were corrected for detector and polarisation efficiency using standard samples (vanadium and amorphous silica, respectively), and have been placed on an absolute scale (barn sr^{-1} Gd^{-1}) by normalising to the incoherent scattering from a vanadium standard. For ordered magnetic and nuclear structures FULLPROF[12] was used to perform Rietveld refinements, with an interpolated background, and instrumental peakshape parameters [10].

B. Computational Details

Computational analyses of our diffuse magnetic neutron scattering data have been performed in a similar way to those undertaken by Paddison *et al.* [13] in their work on GSO. Primary analysis of our data was performed using a mean-field approach

We have used both direct Monte Carlo (DMC) and reverse Monte Carlo (RMC) [14] techniques in order to generate real-space spin-configurations, allowing the direct analysis of the spin-correlation functions along high-symmetry directions, as well as the calculation of the expected single-crystal diffuse magnetic scattering patterns. Reverse Monte Carlo refinements were performed using SPINVERT [17], and direct Monte Carlo simulations were carried out as per ref. [17]. Full computational details of the DMC and RMC analysis are contained in [13, 17, 18].

All our Monte Carlo techniques were made up of $6 \times 6 \times 6$ magnetic unit-cells (containing 3456 spins), and 80 refinement/simulation runs were performed for the purposes of averaging. Since RMC refinements are not dependent on an interaction model, the spin-configurations generated are constrained by: i) the experimental data, ii) the pyrochlore lattice, and iii) a fixed length of Gd^{3+} spins. The stochastic nature of RMC refinements and the random initial spin-configurations produce results which will inherently be as disordered as possible, provided that the above constraints are satisfied.

We have employed the same Hamiltonian for our model-dependent analysis of GPO as that used by Paddison et al. [13] in their analysis of GSO

$$H = -\frac{1}{2}\sum_{i,j} J'_{ij}\hat{\mathbf{S}}_i \cdot \hat{\mathbf{S}}_j + \Delta' \sum_i (\hat{\mathbf{S}}_i \cdot \hat{\mathbf{z}}_i)^2 + \frac{D' r_1^3}{2}\sum_{i,j} \frac{\hat{\mathbf{S}}_i \cdot \hat{\mathbf{S}}_j - 3(\hat{\mathbf{S}}_i \cdot \hat{\mathbf{r}}_{ij})(\hat{\mathbf{S}}_j \cdot \hat{\mathbf{r}}_{ij})}{r_{ij}^3}. \quad (2)$$

This model consists of direct exchange interactions (J'_{ij}) between classical, unit length, spin vectors ($\hat{\mathbf{S}}_i$), single-ion anisotropy (Δ') which is defined by the vector connecting spin i to the centres of the two tetrahedra which both have spin i as a vertex (the local-(111) axis ($\hat{\mathbf{z}}_i$)), and the magnitude, at the nearest-neighbour separation (r_1), of the dipolar interaction (D'). As we have employed a classical Monte Carlo simulation, we have necessarily used parameters relating to the classical unit length spin vectors, denoted by prime superscripts. Comparison between our results and those presented in literature is

facilitated by defining a scaling relationship between classical and quantum parameters.

$$J'_{ij} = J_{ij}S(S+1), \quad (3)$$

$$\Delta' = \Delta S^2, \quad (4)$$

$$D' = DS^2. \quad (5)$$

In classical – S → ∞ – physics, the two scaling factors are identical, whereas at the quantum level there is a difference between the square of the spin projection ($S(S+1)$) and the squared magnitude of the spin (S^2). In the simulations, $D = \mu_0(g\mu_b)^2/4\pi r_1^3 k_b = 0.05275$ K, this is fixed by the lattice parameter $a = 10.225$ Å at 50 mK, and $\Delta = 0.14$ K, determined by interpolation of calculations of the crystal-field levels of $Gd_2Sn_2O_7$ and $Gd_2Ti_2O_7$ – favouring alignment perpendicular to the local-⟨111⟩ axes [19]. In order to minimise the Hamiltonian (2), we have again used a Metropolis algorithm. Long-range dipolar interactions were calculated using Ewald summation, with a simulated metallic boundary. The spin autocorrelation function was calculated from snapshots every $t = 500$ moves, and was checked for correlation, with a value of $\langle \mathbf{S}(0) \cdot \mathbf{S}(t) \rangle \lesssim 0.05$ indicating effective decorrelation of the snapshots. Runs were performed for 5000 moves per spin for equilibration, starting from randomly initialised spin-configurations, and the maximum spin move size was chosen so that approximately 50% of moves were accepted. For direct comparison between the RMC and DMC calculations, the box size for each was chosen to contain $6 \times 6 \times 6$ conventional until cells (3456 spins); in both cases 80 separate calculations were performed in order to statistically average the obtained reciprocal- and real-space correlations.

III. RESULTS

Across all measured temperatures GPO is structurally ordered in the $Fd\bar{3}m$ cubic space group, with a lattice parameter $a \approx 10.225$ Å at 50 mK, in close agreement with previous results.[6] We observe Bragg peaks in the magnetic scattering upon cooling our sample to 50 mK, indicating a transition into an ordered magnetic state. Using FULLPROF we have refined the magnetic scattering and determined that (as per Wills *et al.*[20]) the Γ_7 irreducible representation belonging to a $\mathbf{k} = (0\,0\,0)$ ordering vector provides the best fit to the data. This is the Palmer-Chalker state which has also been observed as the ordered magnetic structure of GSO. Diffraction patterns along with our Rietveld refinements are presented in Figure 2.

The magnetic diffraction from pyrochlore structures often shows broad diffuse-scattering features at temperatures just above the magnetic transition temperature, which arise due to correlated paramagnetism. In order to

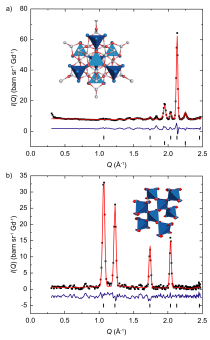

FIG. 2. **a)** Nuclear neutron diffraction pattern and Rietveld fit using a model of GPO. The second set of tick marks are due to the presence of frozen N_2 in our powder. *Inset:* Nuclear structure of GPO showing the pyrochlore network of corner-sharing tetrahedra. **b)** Magnetic neutron diffraction pattern and magnetic Rietveld fit using the Γ_7 irreducible representation (see text). *Inset:* Magnetic structure of GPO, with the Palmer-Chalker state shown as the coplanar antiferromagnetic alignment of the red arrows.

analyse this correlated paramagnetic regime, and hence determine the nature of the interactions leading to the Palmer-Chalker ordered state, we have used both fitting, and modelling techniques. The neutron-scattering data collected at 1.8 K are presented in Figure 3 **b)**. These data show a broad feature centred around $Q \approx 1.1$ Å^{-1} along with a decrease in intensity as $Q \rightarrow 0$, which indicates that strong antiferromagnetic correlations persist over short distances. We have removed a small portion of the data around $Q = 1.8$ Å^{-1} due to spin-leakage in the region of the large nuclear Bragg peak at that position. The analysis of these data was initially performed using a mean-field approximation and a least-squares fitting approach. As illustrated earlier, there are several different exchange pathways in GPO, and in order to produce a model based on a minimal number of parameters, we have performed individual minimisation routines with an increasing number of exchange parameters. These refinements were performed so that the 1.8 K, 4 K, and 200 K datasets were fitted simultaneously. Our χ^2/N_d values for the various refinements and models are presented in

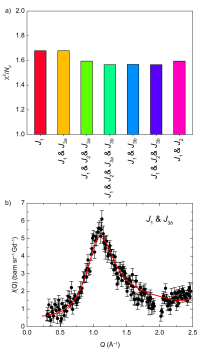

FIG. 3. **a)** χ^2/N_d values for the mean-field models investigated. The inclusion of a J'_{3a} term led in one instance to a non-zero ordering vector, and in all cases refined to zero. **b)** Diffuse magnetic scattering at 1.8 K, as calculated from the mean-field model using J'_1 and J'_{3b}.

Figure 3 **a)**, and the result of our best mean-field model is presented in Figure 3 **b)**. In order to determine the acceptability of the mean-field models we have also calculated the ordering vector with respect to the reciprocal lattice. As stated previously, below T_N $\mathbf{k} = (000)$, and it is reasonable to expect that the ordering vector determined from fitting to paramagnetic data should be close, or equal, to the same $\mathbf{k}$-vector. The inclusion of J_{3a} in our models gives rise to deviations away from this ordering vector, and tends to refine to zero in the mean-field models, therefore it would appear that the parameter is not necessary to model the increased order as the temperature decreases.

In order to extend our analysis beyond mean-field level, we have adopted an 'inverse' Monte Carlo approach, using the values obtained from mean-field fitting as a starting point for a grid search of parameter-space using DMC simulations. As with the mean-field fitting, we observe that a model using only J'_1 does not provide a good fit, while including J'_{3b} provides a much more satisfactory fit. In contrast to mean-field fitting, DMC modelling is a real-space technique, therefore there is a limit to the sharpness of reciprocal-space features that can be modelled (determined by $\Delta Q \simeq 2\pi/r_{max}$, where r_{max} is the largest

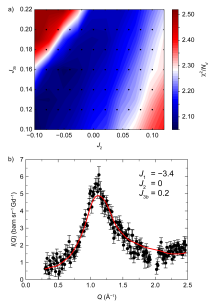

FIG. 4. The results of our DMC modelling based on the values given by mean-filed refinement. **a)** Grid search showing χ^2/N_d for the J'_2, J'_{3b} parameter space. We observe a wide valley of stability for various combinations of the parameters. Visual inspection of the predicted diffuse powder diffraction(**b)**) shows that we can model the local order very well using a minimum model of $J'_1 + J'_{3b}$.

spin separation distance in our model). Our results were checked against $10 \times 10 \times 10$ configurations in order to ensure that box-size constraints do not affect our conclusions. In order to better account for our data, we have followed a similar approach to our mean-field modelling – the systematic inclusion of further-neighbour interaction parameters. Our mean-field results indicate that a model which includes J'_1, and J'_{3b} provides the best realisation of the measured diffuse scattering. Comparison with the phase diagram given in [20] shows that a small, positive, J_2 and a ferromagnetic J_{3b} favours $\mathbf{k} = (000)$. The results of our grid search are presented in Figure 4, where we observe a wide valley of stability for various combinations of the parameters with a two-parameter model giving the best χ^2/N_d for $J'_1 = -3.4$ K, and $J'_{3b} = 0.2$ K. This implies that our powder-averaged data and our modelling approach are sensitive to further-neighbour correlations beyond J'_1 and are not simply a result of including terms beyond mean-field in a J'_1-only model.

We have also compared our mean-field and DMC models to the results of our RMC refinements. As RMC is an inherently stochastic approach, it can be used in order to set a lower bound on the degree of local ordering that is to be expected for the given data – allowed to run for an appropriately long time, RMC will generate the most disordered spin-configuration consistent with the data. The

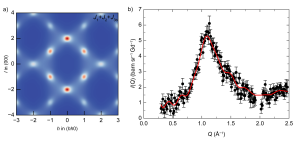

FIG. 5. **a)** Calculated single-crystal diffuse scattering pattern in the hhl-plane for our DMC model with $J_1' = -3.4\,\mathrm{K}$, $J_2' = 0\,\mathrm{K}$, and $J_{3b}' = 0.2\,\mathrm{K}$. As described in the text, we see the intersection of rods of diffuse scattering, giving rise to sharp (diffuse) scattering peaks in reciprocal space. **b)** RMC refinements of this system tend to over-fit the uncertainty in our data, and give rise to narrow peaks in reciprocal-space, implying that there are longer-range correlations than predicted from our DMC modelling.

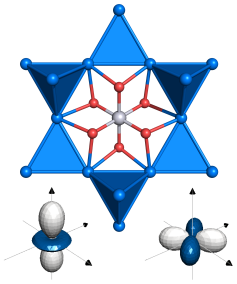

FIG. 6. Pt^{4+} (white sphere) has empty e_g orbitals (in a distorted octahedral environment) allowing superexchange pathways of the form Gd–O–Pt–O–Gd across the hexagonal plane. *Below:* The pseudo-octahedral environment of the Pt^{4+} means that there are e_g orbitals responsible for these pathways.

noise in our data – a consequence of the relatively small sample mass – gives rise to RMC configurations which show long-range correlations (in real space; represented by narrow peaks in reciprocal space). In contrast, the local order is well modelled by the refinement as there is a good fit to the broad peak centred around $Q \approx 1.1\,\mathrm{Å}^{-1}$.

Both of our Monte Carlo approaches give rise to spin-configuration models in real space. From these models, a reciprocal-space map of correlations can be generated in 3D (*i.e.* a single-crystal diffuse-scattering pattern). Across all our models in reciprocal-space we observe rods of diffuse scattering intensity along the [111] directions. These rods intersect, for example, in the (111) and (002) positions, giving rise to intense peaks in a single plane of diffuse scattering. It is at these points in reciprocal space that we observe the development of Bragg peaks in the ordered Palmer-Chalker state. Since the (111) and (002) peaks are strongest in the DMC $J_1' + J_{3b}'$ model, we suggest that this may indicate the development of critical fluctuations associated with the freezing in of antiferromagnetic order [21].

Once we have identified the critical fluctuations responsible for the phase transition, we can investigate the spin-spin correlation functions in particular directions in real space, as defined by:

$$\langle \mathbf{S}(\mathbf{0}) \cdot \mathbf{S}(\mathbf{r}) \rangle = \frac{1}{N} \sum_{i=1}^{N} \sum_{j=1}^{Z_r} \frac{\hat{\mathbf{S}}_i \cdot \hat{\mathbf{S}}_j}{Z_{\mathbf{r}}}. \qquad (6)$$

Figure 7 shows the correlation functions for the high-symmetry directions of the pyrochlore lattice in real space. We have fitted the decay of the correlations using an Ornstein-Zernicke-type function

$$|\langle \mathbf{S}(\mathbf{0}) \cdot \mathbf{S}(\mathbf{r}) \rangle| \approx \frac{1}{|\mathbf{r}|} \exp\left[-\left(\frac{|\mathbf{r}|}{\xi} \right) \right], \qquad (7)$$

where ξ describes the correlation length.

From Figure 7 we can see that along $\mathbf{r}_1$ there are strong antiferromagnetic correlations with a long correlation length of $\xi = 22\,\mathrm{Å}$, along $\mathbf{r}_2$ there are much weaker correlations, which show a general ferromagnetic interaction, but with little decay, and along $\mathbf{r}_{3b}$ there are ferromagnetic correlations which decay with a shorter correlation length than along $\mathbf{r}_1$, $\xi = 9.6\,\mathrm{Å}$.

Despite the similarities between our data and those collected for the closely related GSO, there is a clear difference in the magnitude of the ordering temperature. In GPO the ordering temperature is raised by approximately 60% compared to GSO and GTO. This, in turn, is due to the increased strength of the J_{3b} interaction. Based on previous reports, we propose that the enhancement of the exchange interactions between Gd centres is due to extra superexchange pathways, shown in Figure 6, which are opened up by the presence of empty Pt^{4+}, e_g, orbitals (Gd–O–Pt–O–Gd).

IV. CONCLUSION

We have investigated both the ordered magnetic and the correlated paramagnetic regimes of a ^{160}Gd enriched sample of $Gd_2Pt_2O_7$ using polarised neutron diffraction. These data have been analysed using a combination of mean-field, direct Monte Carlo, and reverse Monte Carlo

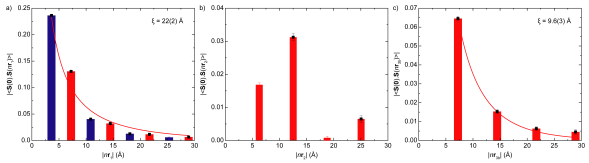

FIG. 7. Spin-spin correlation functions along high-symmetry directions in real space calculated from our best DMC model: **a)** nearest-neighbour vectors $\mathbf{r}_1$ (parallel to J_1), **b)** next-nearest-neighbour vectors $\mathbf{r}_2$ (parellel to J_2), and **c)** 'cross-hexagon' vectors $\mathbf{r}_{3b}$ (parallel to J_{3b}). Black squares show the envelope function of the correlations, red bars show positive correlations, blue bars show negative correlations, and the red lines in **a)** and **c)** show the Ornstein-Zernicke decay according to (7).

techniques. Below T_N we have shown that GPO orders into the Palmer-Chalker state with a $\mathbf{k} = (000)$ ordering vector, as expected based on physical property measurements. Above T_N there is a broad regime of correlated paramagnetic interactions, which give rise to a broad peak of magnetic diffuse scattering. We have used RMC refinement, mean-field modelling, and DMC modelling in order to determine the strength of the exchange interactions which are likely to give rise to the transition into the Palmer-Chalker state at 1.6 K. Since the 'cross-hexagon' (J_{3b}) parameter we observe is much larger than that determined for GSO, we propose that it is the superexchange pathways created by empty Pt^{4+}, e_g-like, orbitals, which give rise to the increased ordering temperature, and hence relieve some of the frustration in the pyrochlore system.

Following on from this work, it would be of interest to measure the single-crystal neutron scattering of GPO as a direct probe of the 'rods' of diffuse-scattering predicted by both RMC refinements and DMC models. This is limited by the availability of single-crystal samples (especially isotope enriched samples). It may also prove instructive to observe the development of these rods as a function of temperature in order to follow the development of the critical fluctuations associated with an antiferromagnetic $\mathbf{k} = (000)$ order. This work may also form the basis of future investigations into similar compounds such as GTO, where the nature of the interactions giving rise to an unusual, partially ordered, ground state, are not fully understood.

[1] L. Balents. Spin liquids in frustrated magnets. *Nature*, 464:199, 03 2010.

[2] J. R. Stewart, G. Ehlers, A. S. Wills, S. T. Bramwell, and J. S. Gardner. Phase transitions, partial disorder and multi- k structures in $Gd_2Ti_2O_7$. *J. Phys.: Condens. Matter*, 16(28):L321, 2004.

[3] C. Castelnovo, R. Moessner, and S. L. Sondhi. Magnetic monopoles in spin ice. *Nature*, 451:42, 01 2008.

[4] R. Moessner and J. T. Chalker. Properties of a classical spin liquid: The heisenberg pyrochlore antiferromagnet. *Phys. Rev. Lett.*, 80:2929–2932, Mar 1998.

[5] R. Moessner and J. T. Chalker. Low-temperature properties of classical geometrically frustrated antiferromagnets. *Phys. Rev. B*, 58:12049–12062, Nov 1998.

[6] A. M. Hallas, A. Z. Sharma, Y. Cai, T. J. Munsie, M. N. Wilson, M. Tachibana, C. R. Wiebe, and G. M. Luke. Relief of frustration in the Heisenberg pyrochlore antiferromagnet $Gd_2Pt_2O_7$. *Phys. Rev. B*, 94:134417, Oct 2016.

[7] X. Li, Y. Q. Cai, Q. Cui, C. J. Lin, Z. L. Dun, K. Matsubayashi, Y. Uwatoko, Y. Sato, T. Kawae, S. J. Lv, C. Q. Jin, J.-S. Zhou, J. B. Goodenough, H. D. Zhou, and J.-G. Cheng. Long-range magnetic order in the Heisenberg pyrochlore antiferromagnets $Gd_2Ge_2O_7$ and $Gd_2Pt_2O_7$ synthesized under high pressure. *Phys. Rev. B*, 94:214429, Dec 2016.

[8] R. Moessner and A. J. Berlinsky. Magnetic Susceptibility of Diluted Pyrochlore and $SrCr_{9-x}Ga_{3+9x}O_{19}$ Antiferromagnets. *Phys. Rev. Lett.*, 83:3293–3296, Oct 1999.

[9] J. R. Stewart, P. P. Deen, K. H. Andersen, H. Schober, J.-F. Barthélémy, J. M. Hillier, A. P. Murani, T. Hayes, and B. Lindenau. Disordered materials studied using neutron polarization analysis on the multi-detector spectrometer, D7. *J. Appl. Cryst.*, 42(1):69–84, Feb 2009.

[10] T. Fennell, L. Mangin-Thro, H. Mutka, G. J. Nilsen, and A. R. Wildes. Wavevector and energy resolution of the polarized diffuse scattering spectrometer D7. *Nucl. Instrum. Methods Phys. Res*, 857:24–30, 2017.

[11] O. Schärpf and H. Capellmann. The xyz-difference method with polarized neutrons and the separation of coherent, spin incoherent, and magnetic scattering cross sections in a multidetector. *Phys. Status Solidi C*, 135(2):359–379, 1993.

[12] J. Rodríguez-Carvajal. Recent advances in magnetic structure determination by neutron powder diffraction. *Physica B: Condens. Matter*, 192(1):55 – 69, 1993.

[13] J. A. M. Paddison, G. Ehlers, O. A. Petrenko, A. R. Wildes, J. S. Gardner, and J. R. Stewart. Spin correlations in the dipolar pyrochlore antiferromagnet $Gd_2Sn_2O_7$. *J. Phys. Condes. Matter*, 29(14):144001, 2017.

[14] R. L. McGreevy and L. Pusztai. Reverse monte carlo simulation: A new technique for the determination of disordered structures. *Mol. Simul.*, 1(6):359–367, 1988.

[15] P. J. Brown. *International tables for crystallography. Volume C*, chapter Magnetic form factors. Dordrecht: Kluwer, 2004.

[16] I. A. Blech and B. L. Averbach. Spin correlations in MnO. *Physics Physique Fizika*, 1:31–44, Jul 1964.

[17] Joseph A. M. Paddison, Ross J. Stewart, and Andrew L. Goodwin. SPINVERT. A program for refinement of paramagnetic diffuse scattering data. *J. Phys.: Condens. Matter*, 25(45):454220:1–15, 2013.

[18] Joseph A. M. Paddison and Andrew L. Goodwin. Empirical magnetic structure solution of frustrated spin systems. *Phys. Rev. Lett.*, 108(1):017204:1–4, 2012.

[19] A. A. Biswas and Y. M. Jana. Estimation of single-ion anisotropies, crystal-field and exchange interactions in Gd-based frustrated pyrochlore anti-ferromagnets $Gd_2M_2O_7$ (M=Ti, Sn, Hf, Zr). *J. Magn. Magn. Mater.*, 323(24):3202 – 3209, 2011.

[20] A. S. Wills, M. E. Zhitomirsky, B. Canals, J. P. Sanchez, P. Bonville, P. D. de Réotier, and A. Yaouanc. Magnetic ordering in $Gd_2Sn_2O_7$: the archetypal Heisenberg pyrochlore antiferromagnet. *J. Phys.: Condens. Matter*, 18(3):L37, 2006.

[21] O. Cépas, A. P. Young, and B. S. Shastry. Degeneracy and strong fluctuation-induced first-order phase transition in the dipolar pyrochlore antiferromagnet. *Phys. Rev. B*, 72:184408, Nov 2005.